Retrieving sub-pixel land cover composition through an effective integration of the spatial, spectral and temporal dimensions of MERIS imagery

Zurita-Milla, Raúl ; Clevers, J G P W ; Schaepman, Michael E ; Plaza, Antonio J

Article ID: 1007-4619(2007)05-0659-10

Retrieving Sub-pixel Land Cover Composition Through an Effective Integration of the Spatial, Spectral and Temporal Dimensions of MERIS Imagery

Raul Zurita-Milla[1], Jan G. P. W. Clevers[1], Michael E. Schaepman[1], Antonio J. Plaza[2]

(1. *Centre for Geo-Information, Wageningen University, P. O. Box 47, 6700 AA Wageningen, The Netherlands*;
2. *University of Extremadura. Computer Science Department, Avda. de la Universidad S/N*, 10.071 *Caceres, Caceres, Spain*)

Abstract: Getting reliable and up-to-date land cover information is essential to model the Earth system. In this respect, the observation capabilities of medium spatial resolution sensors like MODIS or MERIS are offering new land cover mapping possibilities because of the unprecedented resolutions of these sensors. This paper illustrates how the combination of the spatial(300m pixel size), spectral(15 narrow bands in the visible and NIR), and temporal(revisit time 2-3 days) dimensions of MERIS can be used to retrieve sub-pixel fractional land cover composition over heterogeneous areas.

Three MERIS FR Level 1b scenes acquired over The Netherlands in April, July and August 2003 were used to derive fractional composition of the main land cover types present in The Netherlands. A linear spectral unmixing with an optimized number of endmembers per pixel was applied both in a mono- and in a multi-temporal way. A morphological eccentricity index(MEI) was used to explore the MERIS spatial dimension and, subsequently, to support the selection of the endmembers. The Dutch land use database(LGN5), which has a grid structure with a pixel size of 25m, was used as a reference in this study. Classification accuracy was assessed both at per-pixel and at sub-pixel level because of the availability of this high resolution reference data.

The best classification results were obtained for the combined image of April and July with a classification accuracy of about 58%. In general, sub-pixel and per-pixel classification accuracies were found to be similar. Spectral confusion was detected for several classes and dates indicating that the phenological status plays an important role in choosing the optimal combination of acquisition dates and the land cover classes that can be properly identified.

Key words: MERIS; linear spectral unmixing; endmembers; morphology; sub-pixel

CLC number: TP751.1 **Document code**: A

1 INTRODUCTION

1.1 Global land cover mapping

Information on the amount and type of vegetation covering the ground is essential to understand the Earth system because vegetation is a major driver of the energy, water and gas exchanges between the biosphere and the atmosphere[1]. Land cover maps can be used to get this information and, therefore, they are very valuable to model Earth processes like climate change or carbon fluxes[2—4]. Land cover maps are also fundamental to assess the impact of human activities on our environment since anthropogenic land cover change is one of the most important constituents of the socalled "global change"[5]. Despite the importance of reliable and up-to-date land cover maps, the current understanding of the global land cover dy-

Received date: 2006-08-10; **Accepted date**: 2007-03-15

Foundation item: The contribution of R. Zurita-Milla is granted through the Dutch SRON GO programme(EO-061).

Biography: R. Zurita-Milla is currently pursuing the Ph. D. degree at the Centre for Geo-Information of Wageningen University. He works with high and medium spatial resolution (hyperspectral) data. His research interests include: the use of radiative transfer models to retrieve canopy biophysical and biochemical parameters, the extraction of sub-pixel information (fractional land cover composition and continuous fields), image fusion and data assimilation. E-mail: raul.zurita-milla@wur.nl

namics is still far from complete[6]. This is why Earth observation missions have been focusing on land cover mapping since the first acquisitions of remotely sensed data.

The first global land cover maps were derived from the low spatial resolution data provided by the National Oceanic and Atmospheric Administration's (NOAA) Advanced Very High Resolution Radiometer (AVHRR). This sensor pioneered global land cover mapping during the last decades of the previous century although it was primarily designed for meteorological purposes[7]. Due to an increasing interest on global land cover mapping, a new Earth observation instrument specifically designed to monitor the status of the vegetation was launched as a payload of the Système Probatoire de l'Observation de la Terre, SPOT 4 and 5. This instrument, namely VEGETATION(or just VGT), has for instance been used to produce a global land cover map for the year 2000[8]. In addition to these land cover initiatives, temporal series of 1km data provided by the MODerate-resolution Imaging Spectroradiometer (MODIS) have recently been used to produce an updated global land cover map[9].

The coarse resolution ($\geqslant$ 1km) provided by these global land cover initiatives is a limiting factor to map heterogeneous and dynamic areas[10]. Although high spatial resolution sensors could be used to map those areas, their use is not operational at global scales because of their limited spatial extent and low revisit time. This motivated the design and launch of sensors working at medium spatial resolution. Sensors like MERIS (the ESA's MEdium Resolution Imaging Spectrometer) or MODIS are offering this possibility and thus filling the information gap between the high and the low spatial resolution sensors. MERIS and MODIS are able to provide images with a pixel size smaller than 500m. This clearly is an advantage over the $\geqslant$ 1km global datasets provided by the AVHRR and the VGT sensors[11]. Medium spatial resolution sensors are, therefore, providing a new vision of the Earth system because of their unprecedented spatial, spectral and temporal resolutions.

1.2 Sub-pixel land cover mapping

To date, most of the global land cover maps have been produced using per-pixel classification methods[12]. However, per-pixel classification methods do not fully use all the information present in remotely sensed data[13] and, as a consequence, poor classification results have been reported in literature[14]. To overcome this problem, some researchers have introduced sub-pixel classification methods. These methods can be used to retrieve fractional land cover composition and/or to obtain a more detailed description of the vegetation properties(continuous fields). Sub-pixel methods provide information that could otherwise only be acquired by using high resolution data. Moreover, many of the land surface properties that are required to model the Earth system can be better derived using sub-pixel methods than using traditional land cover mapping approaches[13]. Summarising, three main reasons justify the use of sub-pixel land cover methods instead of per-pixel classifiers[10]:

i) Sub-pixel information can be used to detect gradual changes in land cover, both in the spatial and in the temporal domain.

ii) Sub-pixel classification of medium and coarse spatial resolution sensors provide an unbiased estimation of land cover over large areas.

iii) Sub-pixel approaches are theoretically more robust that per-pixel classifiers because they provide a more realistic description of the physics relating land cover to the surface reflectance.

Several sub-pixel methods have been used in literature to retrieve fractional land cover composition or continuous fields: linear spectral unmixing, neural networks, non linear unmixing, fuzzy memberships, empirical relationships between high resolution data and coarse resolution data as well as the following models: probabilistic, geometric-optical and stochastic-geometrical(See Ichoku and Karnieli, DeFries *et al.* and Fernandes *et al.* for a detailed review of these methods)[15,13,10].

In this paper we apply the linear spectral unmixing method, because it is relatively straightforward and computationally fast. Additionally, linear spectral un-

mixing has proven its validity at different spatial scales ranging from coarse to high spatial resolution data[16—19].

1.3 Objective of this paper

The objective of this paper is to evaluate the possibilities of the medium spatial resolution sensor MERIS to retrieve sub-pixel information over(highly) heterogeneous areas using the linear spectral unmixing method. More specifically, the spatial, spectral and temporal resolutions of the MERIS instrument were combined to produce fractional land cover composition maps over the Netherlands. Finally, these maps were validated both at per-pixel and at sub-pixel scales using a high resolution land cover map of the study area.

2 MATERIALS AND METHODS

2.1 MERIS data

The MERIS instrument was launched on board of the ESA's ENVISAT platform in March 2002[20]. MERIS is a fully programmable pushbroom imaging spectrometer that delivers data at 300 m in full resolution mode (FR) and at 1200m in reduced resolution mode (RR). The instrument consists of 5 identical cameras arranged in a fan shape configuration that together provide a 68.5° field-of-view (equivalent to 1150km swath width at nadir). MERIS allows global coverage of the Earth in three days, and since its launch it has been operated with a fixed configuration of 15 spectral bands covering the visible and near infra-red region of the electromagnetic spectrum (Table 1).

Although MERIS was originally designed for oceanographic applications, its potential for land applications was identified prior to its launch[21,22]. Indeed, its fine spectral resolution, its medium spatial resolution, and the high frequency of its acquisitions make MERIS an appropriate sensor to describe most of the land surface processes occurring at regional to global scales.

For this study a set of 3 MERIS FR level 1b (TOA radiance) images acquired over the Netherlands on 16th April, 14th July and 6th August 2003 was used (Fig. 1). Since MERIS is a pushbroom sensor, and the level 1b data is delivered without any spectral preprocessing, the images need to be corrected for the socalled "smile effect"[22]. The Basic ERS & Envisat (A) ATSR and MERIS toolbox, BEAM (smile correction processor version 1.1), was used to perform the smile effect correction.

Table 1 MERIS Band configuration

Band nr.	Band centre/nm	Bandwidth/nm
1	412.5	9.9
2	442.4	10.0
3	489.7	10.0
4	509.7	10.0
5	559.6	10.0
6	619.6	10.0
7	664.6	10.0
8	680.9	7.5
9	708.4	10.0
10	753.5	7.5
11	761.6	3.7
12	778.5	15.0
13	864.8	20.0
14	884.8	10.0
15	899.8	10.0

The three images were subsequently geo-referenced to the Dutch national coordinate system using a nearest neighbour interpolation method. The quality of the geo-location information provided with the images was visually assessed by comparing the geo-referenced images with a vector dataset containing the boundaries of all the Dutch provinces. As a result, a small shift in the image of August was discovered and corrected (this image was co-registered with the other two images). After the geo-referencing, bands 1, 2, 11 and 15 of each image were removed from the analysis because the first two are heavily contaminated by atmospheric scattering (bands in the blue) and the last two fall in absorption features (O_2 and H_2O, respectively). Finally, the images were layer stacked to create a multi-temporal dataset and a cloud free subset of 512 by 256 pixels covering the central part of the country was selected to perform all the analysis.

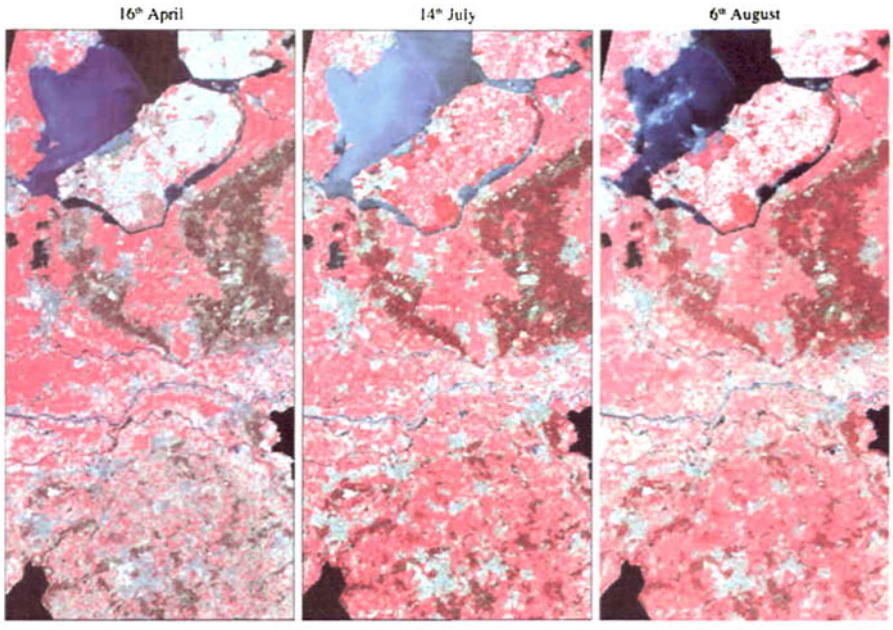

Fig. 1 MERIS FR level 1b images of the study area. (RGB composite using bands 14, 7 and 5)

2.2 Reference data

The latest version of the Dutch land use database, LGN5, was used as reference in this study[23]. The LGN5 has 39 classes, 25 m resolution, and it is based on multi-temporal classification of high resolution satellite data and integration of ancillary data. Due to its recent completion (June 2005), the overall classification accuracy of the LGN5 is still to be determined. Preliminary results indicate that the classification accuracy of the LGN5 will be similar to the one of the previous version (LGN4) which was between 85% and 90% depending on the land cover type. The original 39 classes of the LGN5 were aggregated into 9 main land cover classes: grassland, arable land, greenhouses, deciduous forest, coniferous forest, water, built-up areas, bare soil (mainly sand dunes), and natural vegetation. Next, a spatial aggregation (based on a majority filter) was applied to match the 300 m pixel size of the MERIS FR scenes. During the spatial aggregation process, the fractions of the different land cover types present in each MERIS pixel were computed so that a sub-pixel validation of the estimated fractional land cover composition could be done. Finally, the LGN5 dataset was "clipped" to the same extent as the MERIS images (512 by 256 pixels).

2.3 Selection of the endmembers

Most of the methods that have been proposed in literature for the selection of pure land cover spectra or endmembers, rely on the spectral information present in the image and, generally, do not make use of the spatial information of the image that is going to be unmixed. In this paper, a spatial and spectral endmember extraction method called automated morphological endmember extraction (AMEE) was used[24]. The AMEE method is based on the use of the multidimensional erosion and dilation operations[25]. Multidimensional erosion selects the pixel vector most similar (in spectral sense) to its spatial neighbours, while multidimensional dilation selects the most spectrally unique ("pure") pixel vector of the selected neighbourhood. The main outcome of the AMEE method is a morphological eccentricity index (MEI) defined at a pixel level. In this study, the values of this index are used to define spatially homogeneous areas from where the endmembers will be collected. The MEI is calculated as the spectral angle distance between each pixel and

the average signature (most highly mixed one) in the surroundings of that pixel. As a result, low MEI values generally belong to pixels situated in spectrally homogeneous areas whereas high MEI values are assigned to the purest pixels in the spatial neighbourhood.

In this study, we computed the MEI for each MERIS scene and for the multi-temporal dataset using a sliding window of 3 by 3 pixels. After that, a threshold over the MEI values was set in order to define potential areas to search for endmembers. This threshold was empirically fixed to the lowest 10% values. Because the classes greenhouse and bare soil occupy a very small proportion of the total surface (0.11% and 0.23%, respectively), we empirically set a second threshold to the upper 10% of the MEI values so that we could identify pixels belonging to these small and fragmented classes.

Pixels that were labelled as potential candidates to become endmembers were then grouped by class using the aggregated version (300m) of the LGN5 as a reference. After this, an outlier removal algorithm namely the Grubbs' test[26] was applied to each group. A final set of endmembers was generated by averaging the remaining pixels.

2.4 Spectral unmixing

Linear spectral unmixing (LSU) was used to derive fractional land cover composition maps from the available MERIS images. LSU methods assume that there is no multiple scattering occurring within the different land cover types. In that case, the signal received per pixel is just a linear combination of the signals corresponding to "pure" land cover types weighted by their area within the pixel (Eq. 1). Let *nb* and *nc* represent the number of bands and classes respectively, then:

$$pv_i = \sum_{c=1}^{nc} (f_c \cdot \mu_{ci}) + e_i \quad i = 1,2,\cdots,nb \quad (1)$$

Where, pv_i is the pixel value for the band-i, f_c is the fraction of the land cover-c present in that pixel, μ_{ci} is the pure signal of the land cover-c in the band-i, and e represents the errors due to (sensor) noise.

Several LSU approaches are available in literature: constrained, unconstrained or partially constrained[27]. In this study, the unmixing method described by Ramsey and Christensen will be used[28]. This method iteratively optimizes the number of endmembers that are used to retrieve the fractional composition of each pixel. An unconstrained least squares inversion is first performed for each pixel. After this, the endmembers that yielded negative abundances are removed from the analysis of that pixel. This process is iteratively repeated until no negative fractions are found and then the retrieved fractions are rescaled to fulfil the two classical constraints that ensure the physical interpretation of the results: fractions must be positive and below 1 and the sum of all the fractions must add to unity (Eq. 2).

$$0 \leqslant f_c \leqslant 1 \text{ and } \sum_{c=1}^{nc} f_c = 1.0 \quad (2)$$

This iterative unmixing method was preferred because the algorithm is not "forced" to find abundances for all the endmembers in each pixel. Additionally, the removal of endmembers that yield negative fractions might result in a reduction of the spectral confusion of the remaining endmembers. In contrast, the residual errors might increase since the inversion will be performed with a limited number of endmembers[28]. Nonetheless, no large residuals are expected because no constraint is imposed during the least-squares inversion.

The iterative LSU was rewritten in a matrix-vector notation (Eq. 3) and it was implemented in MATLAB®.

$$\boldsymbol{PV}_{(nbx1)} = \boldsymbol{M}_{(nbxnc)} \cdot \boldsymbol{F}_{(ncx1)} + \boldsymbol{E}_{(nbx1)} \quad (3)$$

$\boldsymbol{PV}$ is now the vector storing the MERIS radiance values per pixel, $\boldsymbol{M}$ is the matrix containing the spectra of the endmembers, $\boldsymbol{F}$ is the vector of the fractions or abundances that we seek and finally, $\boldsymbol{E}$ is the vector of residual errors.

Two outputs are traditionally provided by the LSU methods: the sub-pixel fractional land cover composition, $\boldsymbol{F}$, and the spectral root mean square error (RMSE) computed from the vector of errors $\boldsymbol{E}$. The selected approach offers, however, an "extra" output: the number of endmembers effectively used to unmix every pixel. This output can be obtained be-

cause as explained above the size of the matrix M is iteratively optimised for each pixel.

The selected iterative LSU was applied to both the mono- and the multi-temporal MERIS FR datasets. The unmixing of the multi-temporal image (or temporal unmixing) was selected because in this way the different land cover types will not only be defined by their spectral signatures, but also by their temporal profile. If the appropriate dates are selected, the temporal unmixing should increase the discrimination of spectrally similar land cover types.

2.5 Accuracy assessment

An extensive accuracy assessment of the unmixing results was done both at sub-pixel and per-pixel level. Assuming that the estimated fractions are correctly positioned within the pixel, the overall sub-pixel accuracy can be computed as follows:

$$OSA = \sum_{c=1}^{nc} d_c \Big/ \sum_{c=1}^{nc} f_c^* = \sum_{c=1}^{nc} d_c \qquad (4)$$

$$d_c = min\{f_c^{LGN5}, f_c^*\} \quad c = 1,2,\cdots,nc$$

where: OSA is the overall sub-pixel accuracy for a given pixel-p, d_c are the correctly classified fractions for class-c and pixel-p (the diagonal elements of the confusion matrix), and f_c^{LGN5} are the LGN-based fractional abundances of class-c in the pixel-p. Notice that f_c^* is subject to Eq. 2 and that, therefore, it adds to unity. Finally, a mixed-to-pure-pixel-converter based on a majority rule was applied to the fractional images to generate "hard" classification maps. The accuracy of these maps was subsequently evaluated using a confusion error matrix and the kappa coefficient.

3 RESULTS

The spectral signature of the main land cover types of The Netherlands was computed for each MERIS date as an average of the pixels identified using the MEI. As an example, Fig. 2 illustrates the endmembers for the image of the 16th of April.

The shape of the endmembers corresponds to the typical spectra of the respective classes when these are measured at the TOA radiance level. This is, the first bands show a relatively high reflectance due to atmospheric scattering and the vegetation classes show a steep slope between the red and NIR bands.

The image of August, followed by the one of July, presented the highest spectral confusion among the endmembers. Grassland and arable land, which are the two main land cover types in the study area, were the classes most frequently confused. This spectral

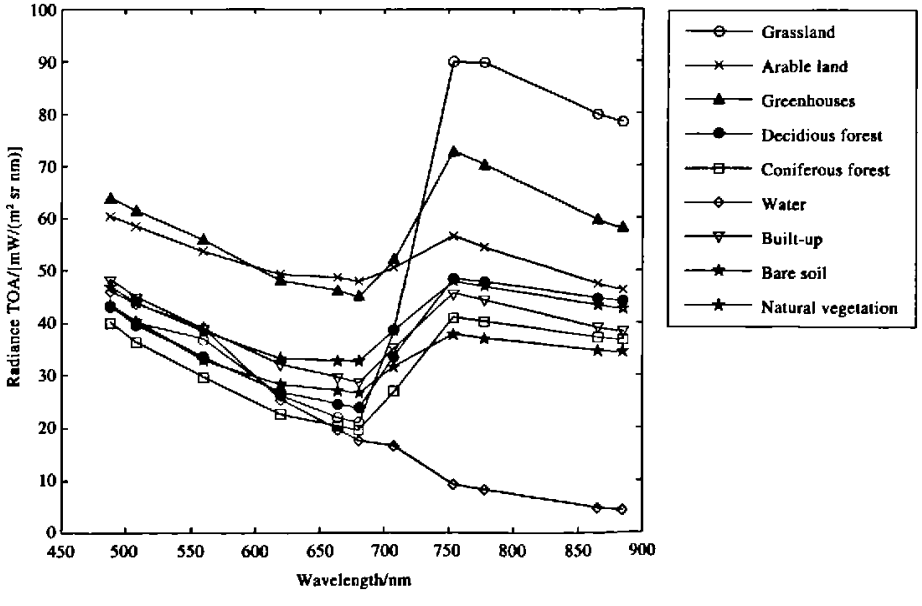

Fig. 2 Endmembers for the 16th of April 2003

confusion can be explained by the relatively high withinclass variability in this period. For instance, grasslands have different management practices during the growing season and, therefore, a higher spectral variation in summer. Furthermore, the class arable land comprises a multitude of crop types, which naturally leads to a combination of different spectral signatures. Additionally, a single crop can have distinct planting and harvesting dates on different fields and as a consequence, the different growth stages further diversify the crop spectral signature.

The iterative spectral unmixing resulted in 9 images containing the fractional abundances of the main land cover types, an image showing the spectral RMSE, and an image showing the number of endmembers that were used to unmix every pixel. By comparing this last image with the number of classes present in each (300m aggregated) pixel of the LGN5, it was concluded that the number of endmembers used during the unmixing was adequately identified.

A visual analysis of the spectral RMSE images obtained for the mono- and multi-temporal unmixing did not reveal any kind of spatial pattern in these images. This indicates two issues: (i) that the selected endmembers are representative of the land cover types present in the study area and therefore they can be used to unmix the images, and (ii) that despite the fact that we are working with MERIS 11b data (TOA radiances), no atmospheric effect (e. g. aerosols) significantly hampered the unmixing. This was somehow expected because the study area is relatively small (and therefore it can be approximated by one atmosphere) and because the endmembers are the average of several pixels more or less distributed over the whole scene.

Looking at the fractional abundance images and the "hard" classified maps that were derived from these images we decided to merge the classes built-up and greenhouses into a single built-up class. After this thematic aggregation, an extensive accuracy assessment was done for all the MERIS images both at a sub-pixel and at a per-pixel level. Table 2 summarises the results of this accuracy assessment.

The best classification results were obtained for the combined image of April and July followed by the image of April. This indicates the necessity of defining appropriate rules for the optimal selection of the dates that should be used in a temporal unmixing because increasing the number of dates does not imply higher classification accuracy. The use of phenological information collected over the study area might help to define the best dates for a temporal unmixing.

Table 2 Accuracy assessment

	MSA/%	*OA*/%	*Kappa*
16th April	55.37(33.27)	55.38	0.461
14th July	49.42(34.22)	49.43	0.391
6th Aug	48.94(33.95)	49.61	0.390
16th April + 14th July	57.79(30.27)	58.03	0.486
16th April + 14th July + 6th Aug	47.84(33.55)	47.72	0.375

MSA: mean sub-pixel classification accuracy; *MSA* standard deviation values are shown between brackets;
OA: overall classification accuracy.

Fig. 3 illustrates the reference data aggregated to 300m and 8 classes (left) and the "hard" classified image obtained from the April + July combined image (right). By comparing these two figures we can see that most of the misclassifications are situated in the

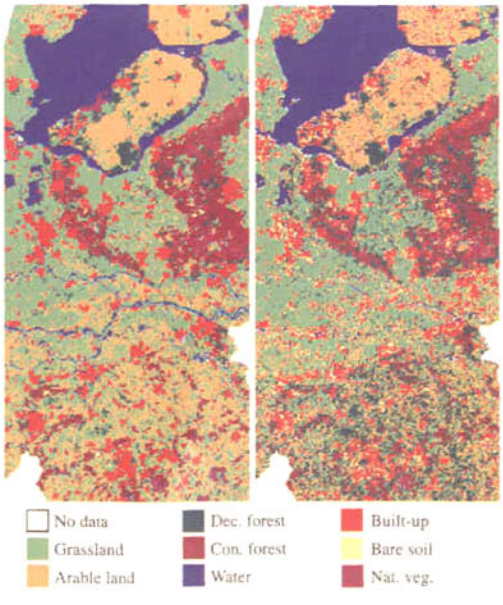

Fig. 3 LGN5 (left) and hard classification of the April + July image (right)

southern part of the study area, which is a very fragmented region.

The confusion matrix and the user's and producer's accuracies of this combined image of April and July are given in Table 3. Water, grassland and coniferous forest are the classes with the highest user's accuracies. Furthermore, this table shows that the class arable land is difficult to map at medium spatial resolution, as this class is very heterogeneous (different crops and different planting/harvesting dates). Thus, nearly half of the pixels classified as arable land belong to other land cover types. Finally, the classes bare soil and deciduous forest present the worst user's accuracies.

Table 3 Confusion matrix for the 16th April + 14th July image

Classification result	Reference dataset (LGN5)								UA/%
	GL	AL	DF	CF	W	B	BS	NV	
GL	**27188**	5033	535	355	381	825	6	20	79.17
AL	6053	**13051**	522	440	881	1796	13	378	56.41
DF	5754	5248	**3588**	3475	566	1173	11	329	17.81
CF	439	248	515	**6711**	121	311	9	245	78.04
W	256	47	33	28	**12994**	184	21	92	95.16
B	3983	2630	519	972	484	**8991**	73	387	49.84
BS	2020	855	99	135	419	1717	**146**	164	2.63
NV	455	745	137	638	58	567	17	**1178**	31.04
PA/%	58.91	46.85	60.32	52.62	81.70	57.77	49.32	42.18	

The sub-pixel classification accuracy for the combined image of April and July is illustrated in Fig. 4. Water has the best mean sub-pixel classification accuracy followed by grassland. However, most of the classes present a large variation in sub-pixel accuracy (Table 2). Bare soil and natural vegetation were the two worst classified classes.

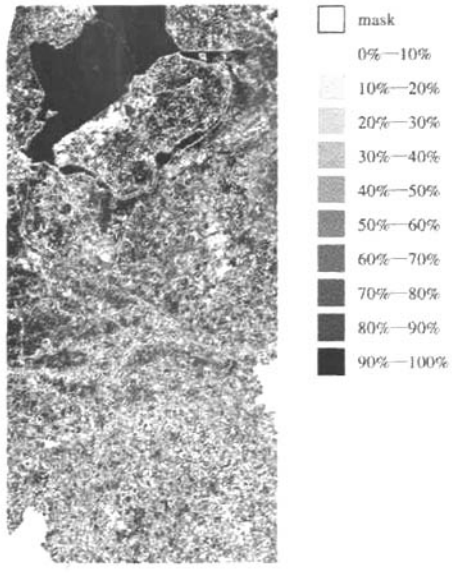

Fig. 4 Sub-pixel classification accuracy for the April + July image

4 CONCLUSIONS

In this paper we have demonstrated that through an effective integration of the spatial, spectral and temporal dimensions of MERIS imagery it is possible to retrieve fractional land cover composition at regional scale. Classification results indicate that the use of morphological operations to derive pure spectral signatures using both spatial and spectral information is very promising. In addition to this, the linear spectral unmixing with an optimized number of endmembers has also proven to be effective to retrieve fractional land cover composition (especially considering the number of endmembers and their spectral separability). However, the selection of the number of dates to be used in the temporal unmixing needs to be optimized because increasing the number of dates does not automatically imply better classifications. We suggest to explore the role of vegetation phenology to find the best combination of dates for a temporal unmixing.

For the best classified image, the combined image of April and July, the overall sub-pixel classification accuracy reached 58.03%. Results after "hardening" the classifications by assigning to each pixel the label of the class presenting the highest fractional coverage were similar to the ones obtained during the sub-pixel analysis. This confirms the validity of the fractional land cover maps and favours the use of sub-pixel methods since they offer more information than traditional per-pixel classifiers. This "extra" information could be used, for instance, to monitor sub-pixel land cover changes.

Finally, the findings presented in this study should support the use of soft classifiers to map very heterogeneous and fragmented areas with medium and low spatial resolution sensors like NOAA/AVHRR, SPOT/VGT, MODIS and MERIS.

REFERENCES

[1] Sellers P J, Dickinson R E, Randall D A, *et al*. Modeling the Exchanges of Energy, Water, and Carbon between Continents and the Atmosphere[J]. *Science*, 1977, **275**(5299): 502—509.

[2] Brovkin V, Ganopolski A, Claussen M, *et al*. Modelling Climate Response to Historical Land Cover Change[J]. *Global Ecology and Biogeography Letters*, 1999, **8**(6): 509—517.

[3] Gutman G, Janetos A C, Justice C O, *et al*. Land Change Science: Observing, Monitoring and Understanding Trajectories of Change on the Earth's Surface[M]. Berlin (Germany), Springer-Verlag, 2004.

[4] Plummer S, Arino O, Fierens F, *et al*. The GLOBCARBON Initiative: Multi-sensor Estimation of Global Biophysical Products for Global Terrestrial Carbon Studies. European Space Agency, (Special Publication)[A]. ESA SP[C]. 2005, (572): 1197—1204.

[5] Vitousek P M. Beyond Global Warming: Ecology and Global Change[J]. *Ecology*, 1994, **75**(7): 1861—1876.

[6] Foody G M. Status of Land Cover Classification Accuracy Assessment[J]. *Remote Sensing of Environment*, 2002, **80**(1): 185—201.

[7] Townshend J, Justice C, Li W, *et al*. Global Land Cover Classification by Remote Sensing: Present Capabilities and Future Possibilities[J]. *Remote Sensing of Environment*, 1991, **35**(2—3): 243—255.

[8] Bartholomé E, Belward A S. GLC2000: A New Approach to Global Land Cover Mapping from Earth Observation Data[J]. *International Journal of Remote Sensing*, 2005, **26**(9): 1959—1977.

[9] Friedl M A, McIver D K, Hodges J C F, *et al*. Global Land Cover Mapping from MODIS: Algorithms and Early Results[J]. *Remote Sensing of Environment*, 2002, **83**(1—2): 287—302.

[10] Fernandes R, Fraser R, Latifovic R, *et al*. Approaches to Fractional Land Cover and Continuous Field Mapping: A Comparative Assessment over the BOREAS Study Region[J]. *Remote Sensing of Environment*, 2004, **89**(2): 234—251.

[11] Justice C O, Markham B L, Townshend J R G, *et al*. Spatial Degradation of Satellite Data[J]. *International Journal of Remote Sensing*, 1989, **10**(9): 1539—1561.

[12] Franklin S E, Wulder M A. Remote Sensing Methods in Medium Spatial Resolution Satellite Data Land Cover Classification of Large Areas[J]. *Progress in Physical Geography*, 2002, **26**(2): 173—205.

[13] DeFries R S, Hansen M C, Townshend J R G. Global Continuous Fields of Vegetation Characteristics: a Linear Mixture Model Applied to Multi-year 8km AVHRR Data[J]. *International Journal of Remote Sensing*, 2000, **21**(6—7): 1389—1414.

[14] Friedl M A, Woodcock C, Gopal S, *et al*. A Note on Procedures Used for Accuracy Assessment in Land Cover Maps Derived from AVHRR Data[J]. *International Journal of Remote Sensing*, 2000, **21**(5): 1073—1077.

[15] Ichoku C, Karnieli A. A Review of Mixture Modeling Techniques for Sub-pixel Land Cover Estimation[J]. *Remote Sensing Reviews*, 1996, **13**: 161—186.

[16] Foppa N, Wunderle S, Hauser A. Operational Snow Cover Estimation at Subpixel Scale Using NOAA-AVHRR Data[A]. Proceedings of SPIE-The International Society for Optical Engineering, 2002.

[17] Lobell D B, Asner G P. Cropland Distributions from Temporal Unmixing of MODIS Data[J]. *Remote Sensing of Environment*, 2004, **93**(3): 412—422.

[18] Settle J J, Drake N A. Linear Mixing and the Estimation of Ground Cover Proportions[J]. *International Journal of Remote Sensing*, 1993, **14**(6): 1159—1177.

[19] Smith M O, Ustin S L, Adams J B, *et al*. Vegetation in Deserts: I. A Regional Measure of Abundance from Multispectral Images[J]. *Remote Sensing of Environment*, 1990, **31**(1): 1—26.

[20] Rast M, Bezy J L, Bruzzi S. The ESA Medium Resolution Imaging Spectrometer MERIS-a Review of the Instrument and Its Mission[J]. *International Journal of Remote Sensing*, 1999, **20**: 1681—1702.

[21] Verstraete M M, Pinty B, Curran P J. MERIS Potential for Land Applications[J]. *International Journal of Remote Sensing*, 1999, **20**(9): 1747—1756.

[22] Zurita-Milla R, Clevers J G P W, Schaepman M, Kneubuehler M. Effects of MERIS L1b Radiometric Calibration on Regional Land Cover Mapping and Land Products[J]. *International Journal of Remote Sensing*, 2007, **28**(3—4): 653—673.

[23] Hazeu G. The Dutch Land Use Database LGN. [web page] http://www.lgn.nl/[accessed 22nd February 2006].

[24] Plaza A, Martínez P, Pérez R, *et al*. Spatial/spectral Endmember Extraction by Multidimensional Morphological Operations [J]. *IEEE Transactions on Geoscience and Remote Sensing*, 2002, 40(9): 2025—2041.

[25] Plaza A, Martínez P, Plaza J, *et al*. Dimensionality Reduction and Classification of Hyperspectral Image Data Using Sequences of Extended Morphological Transformations[J]. *IEEE Transactions on Geoscience and Remote Sensing*, 2005, 43(3): 466—479.

[26] Beckman R J, Cook R D. OUTLIER..... S. *Technometrics*, 1983, 25(2): 119—149.

[27] Chang C I. Hyperspectral Imaging: Techniques for Spectral Detection and Classification, Springer/Kluwer, New York, 2003.

[28] Ramsey M S, Christensen P R. Mineral Abundance Determination: Quantitative Deconvolution of thermal Emission Spectra [J]. *Journal of Geophysical Research B: Solid Earth*, 1998, 103(1): 577—596.

基于 MERIS 影像空间、光谱及时间维信息提取亚像元级的土地覆盖组分

Raul Zurita-Milla[1], Jan G. P. W. Clevers[1], Michael E. Schaepman[1], Antonio J. Plaza[2]

(1. 瓦赫宁根大学地理信息中心, P. O. Box 47, 6700 AA 瓦赫宁根, 荷兰;
2. 埃斯特雷马杜拉大学计算机科学系, Avda. de la Universidad S/N, 10.071 西班牙)

摘 要: 及时获取有效的土地覆盖信息是地球系统模拟的基础。因此,中等空间分辨率传感器如 MODIS 或 MERIS 空前的通道设置与观测能力,使其具有快速更新土地覆盖图的能力。本文说明了如何结合 MERIS 的空间维(像元大小为 300m)、光谱维(可见光与近红外范围内 15 个通道)和时间维(重返周期 2—3d),用于获取不同区域土地覆被组分的亚像元级组成权重。利用 4 月、7 月和 8 月三期 MERIS FR 1b 级数据得到荷兰主要土地覆被类型的组成权重。单一时相和多时相的数据都使用单个像元最优化的端元数进行线性光谱分解。利用一种形态偏离指数得到 MERIS 的空间维并用于端元的选择。应用荷兰土地利用数据库(LGN5)25m 分辨率的栅格数据作为本文的参考数据。基于这种数据的高分辨率,因此可以从像元和亚像元的水平同时评价的分类精度。

结果显示,结合 4 月和 7 月的影像可以获得最优的分类结果,精度约为 58%。总的说来,亚像元和像元级的分类精度相似。通过几种组分类别和日期的光谱融合表明,物候状况对于数据获取时相最佳结合的选择以及正确识别土地覆盖类型的重要性。

关键词: MERIS; 线性光谱分解; 端元; 形态学; 亚像元